

Additional Acceleration of Protons and Energetic Neutrino Production in a Filamentary Jet of the Blazar Markarian 501

Yasuko S. HONDA

*Department of Total Systems Engineering, Kinki University Technical College,
Kumano, Mie 519-4395*

yasuko@ktc.ac.jp

Mitsuru HONDA

Plasma Astrophysics Laboratory, Institute for Global Science, Kumano, Mie 519-4327

(Received 2009 July 19; accepted 2010 April 6)

Abstract

Blazars have been regarded as one of the most powerful sources of the highest energy cosmic rays and also their byproducts, neutrinos. Provided that a magnetized filamentary system is established in a blazar jet as well, we could apply the mechanism of multi-stage diffusive shock acceleration to a feasible TeV emitter, Mrk 501 to evaluate the achievable maximum energy of protons. Taking conceivable energy restriction into account systematically, it seems adequate to say that EeV-protons are produced at this site by our present model. We also estimate neutrino fluxes generated by these accelerated protons and discuss the detectability based on an updated kilometre-scale telescope such as IceCube.

Key words: galaxies: individual (Markarian 501) — magnetic fields — methods: numerical — neutrinos: individual (Markarian 501) — shock waves

1. Introduction

The origin of the ultra-high energy cosmic rays (UHECRs) beyond 100 EeV has still been an enigma in modern astrophysics. UHECRs are frequently accompanied by significant fluxes of energetic neutrinos generated in processes associated with hadronic interactions. Although the source direction of cosmic rays with energy above 60 EeV can be identified by an analysis of recent Auger data (Abraham et al. 2007), neutrinos are regarded as being the most useful probe of their source confirmation owing to no deflection by galactic/intergalactic magnetic fields and the weakest reduction by interactions with the cosmic background radiation. The

models for the origin of the highest energy cosmic rays are classified into two categories: top-down and bottom-up. In top-down scenarios, neutrinos are presumed to be decay or annihilation products of cosmological remnants with the Grand Unified energy scale of $\sim 10^{15}$ GeV. Within this framework, numerous models have been proposed so far, such as topological defects, Z-bursts, annihilation of dark matter particles and so on (for a review, see Bhattacharjee & Sigl 2000). In an alternative approach, the bottom-up model is based on the idea that the highest energy cosmic rays are generated by astrophysical objects. The most plausible candidates are gamma ray bursts (GRB: Waxman & Bahcall 1997; Vietri 1998) and active galactic nuclei (AGN: Honda & Honda 2004a; Honda 2009). In addition to these objects, it is pointed out that UHECRs are also produced via stochastic acceleration in the giant lobes of radio galaxy (Cen A: Frascetti & Melia 2008; O’Sullivan et al. 2009), which accounts for the past year discovery by the HiRes and Auger collaborations. Supernova remnants, X-ray binaries, mini-quasars (e.g. Gaisser, Halzen, & Stanev 1995, for a review), and soft gamma ray repeaters (SGR: Halzen et al. 2005; Ioka et al. 2005) can also be stellar type neutrino sources, any of which could produce observable fluxes of energetic neutrinos. If protons are accelerated at these astrophysical objects, neutrinos are expected to be produced in collisions with ambient photons or protons.

Some of the above-mentioned models predict neutrino flux at the level of a few events per km^2 year. The upper range of this estimation seems to be within reach of a first-generation neutrino telescope, such as AMANDA (Antarctic Muon And Neutrinos Detector Array). Among a wide variety of physics topics to be explored with the neutrino telescope, the most important goal is to search for the origin of cosmic radiation, especially that originated from AGN and/or GRB. For this purpose, AMANDA has been primarily optimised in the energy range from TeV to PeV, targeting not only the diffuse, but point source, flux of energetic neutrinos. According to an analysis of AMANDA data, we unfortunately have no evidence for point sources so far, (Woschnagg et al. 2005; Abbasi et al. 2009), except for a temporal coincidence with an orphan flare of the TeV blazar, 1ES 1959+650 (Halzen & Hooper 2005). The IceCube, a cubic kilometre-scale neutrino telescope, which is partly operating and still under construction as a successor to AMANDA at the same site, is designed to detect the fluxes about 10-50 events per km^2 year. Similar event rates are predicted by model calculations assuming that AGN or GRB are the actual source (Halzen 2005) and hence the IceCube is expected to certainly detect neutrino fluxes from such point sources. In order to observe a *guaranteed* source, however, even the km^3 -sized detector should safely operate over a period of at least ten years.

As for the cosmic accelerators, the most promising mechanism to lead highest energies and power-law energy spectrum is considered to be of diffusive shock acceleration (DSA: Drury 1983; Lagage & Cesarsky 1983a; 1983b). Solar energetic particles and galactic cosmic rays are consistently explained by this mechanism applied to shocks at heliosphere and supernova remnants, respectively (for a review, see Blandford & Eichler 1987); these acceleration sites have

actually been confirmed by some observations (Koyama et al. 1995). Polarization data in the range of radio to optical wavelengths imply that *in situ* acceleration of electrons (and possibly ions) must also be taking place in the knots of AGN jets (Honda & Honda 2004a) or in the hot spots of Fanaroff-Riley type-II (FR-II) sources (probably terminal shocks) (Perley et al. 1984; Carilli & Barthel 1996). At these sites, magnetic fields in the vicinity of a shock front plays an essential role in particle acceleration. A detailed configuration of the fields in extragalactic jets has been revealed by polarization measurements using very long-baseline interferometry. For example, the quite smooth fields predominantly transverse to the jet axis, are typically observed in the core region of BL Lac objects (1803+784: Gabuzda 1999; 0300+470: Nan et al. 1999). Allowing the propagation of a shock wave through the jets, this implies the establishment of a (quasi-) perpendicular shock, which is capable of accelerating cosmic ray particles efficiently. Evidence for large-scale toroidal magnetic fields has been also discovered in the galactic center (GC) region (Novak et al. 2003). Based on the above results, it seems adequate that system of magnetized filaments has been established in blazar jets as well.

We have suggested a theoretical model to account for the generation of such a large-scale toroidal (transverse) magnetic field in astrophysical jets (Honda & Honda 2002). In this model, huge currents launched from a central engine are broken into many filaments whose transverse sizes are self-adjusted for the electromagnetic current filamentation instability (CFI: Honda 2004 and references therein). In the nonlinear stage of the CFI, the magnetized filaments are often regarded as being strong turbulence that can largely deflect charged particles. Allowing shock propagation through the jet, the particles are expected to be quite efficiently accelerated for the DSA scenario, which appears to be favorably taking place in the AGN jets. Indeed, some knots of a radio galaxy jet are associated with the shock fronts (M87: Biretta et al. 1983; Capetti et al. 1997) and circumstantial evidence for in-situ acceleration of electrons (Meisenheimer et al. 1989) have been found. It was also pointed that a similar pattern of small-scale quasi-static magnetic fields can also be established by some numerical simulations: e.g., during the collision of electron-positron plasmas existing in SNRs, pulsar winds, GRBs, relativistic jets, and so on (Kazimura et al. 1998; Silva et al. 2003). Using a three-dimensional relativistic electromagnetic code, Nishikawa (2003) show that non-uniform small-scale magnetic field is generated due to the Weibel instability at a jet front propagating through an ambient plasma with/without initial fields. These dynamics might be involved in some of the knots in the FR-I radio jets, which appear to be a shock established when faster material is overtaking with slower one (M87: Biretta et al. 1983).

In the case of blazars, however, the detailed internal structure of their jets has still not been confirmed because of optical thickness with respect to the observer's line of sight. Another approach to shed light on their configuration is provided by the remarkable short variability timescale of a blazar light curve (e.g., Mrk 421: reaching a few minutes, Cui 2004; Blazejowski et al. 2005). This is significantly shorter than the light-crossing time at the black hole horizon,

which implies the presence of some substructure in the parsec-scale jet. According to our model configuration of the filamentary jet, the strength of the local magnetic field is described by a power-law of the filaments transverse sizes. If charged particles are injected into this system, they are diffusively accelerated by a collisionless shock being scattered by the field fluctuations. Since the efficiency of the acceleration and loss depends upon the spatial size scales, the local maximum energies of accelerated particles are also characterized by their nearest filament sizes. The spectrum extending to the X-ray region is attributed to the synchrotron radiation of accelerated electrons. In particular, the correlation between X-ray and gamma-ray light curves of Mrk 421 is well reproduced by a model of the hierarchical turbulent structure of the jet (Honda 2008). The most interesting consequence is that the transition of a hierarchical turbulent structure seems to be responsible for the observed patterns of energy-dependent light curves, e.g., soft lag (Takahashi et al. 1996; Rebillot et al. 2006) or hard lag (Fossati et al. 2000) and a tight-correlation mode (Sembay et al. 2002).

As for Mrk 501, which is also firmly established as a TeV γ -ray emitter, the X-ray light curve shows a very rapid flare varying over several 100 seconds (Catanese & Sambruna 2000). It is also revealed that the TeV flares correlate with X-ray radiation on timescales of hours or less from multiwavelengths observations (Pian et al. 1998; Catanese et al. 1997; Krawczynski et al. 2000; Sambruna et al. 2000). Moreover, the largest shift of the peak energy during the peak-luminosity change was observed among all blazars (Kataoka et al. 2001). Summarizing these observational results, we can say that the acceleration of electrons similar to Mrk 421 is also taking place in Mrk 501. Presuming a finite ion abundance in the jet of Mrk 501 (Rawlings & Saunders 1991), such a DSA mechanism operates for arbitrary nuclei (of course including protons) as well. Indeed, from the X-ray spectrum of SS 433 jet, emission lines of various elements such as Ne, Mg, Si, and Fe were observed (Kotani et al. 1996).

In the present paper, we evaluate the achievable maximum energy of protons in the Mrk 501 jet to estimate the resultant neutrino fluxes in accordance with our diffusion and acceleration mechanism in a filamentary jet, which we have proposed and developed in a series of papers (Honda & Honda 2004b; 2005; 2007). In section 2, installing our model structure of magnetized filaments to the jet of Mrk 501, we describe the acceleration processes of protons using our novel DSA mechanism. Taking competitive energy losses and restrictions into consideration, we present the scaling of the maximum energy. In §2.1 we describe the acceleration taking place at local magnetic fields induced by the current filament each (referred to as preliminary acceleration) and in §2.2 the additional acceleration due to the inter-filaments' deflection. In §2.3, we calculate the achievable maximum energies of accelerated protons with respect to the transverse filament sizes and magnetic field parameters. We then evaluate neutrino flux from Mrk 501 and discuss its detectability based on a km-scale neutrino telescope such as IceCube in section 3. Conclusions are summarized in section 4.

2. Proton Acceleration in Magnetized Filaments

Suppose a parsec-scale blazar jet transporting energetic particles from the central engine. The directional plasma flow will favorably induce huge currents (Appl & Camenzind 1992) that breaks up into many filaments because of electromagnetic CFI. Each filament generates a small-scale transverse magnetic field whose strength is determined by the transverse size of a filament, λ , i.e., $|\mathbf{B}| = B_m(\lambda/D)^{(\beta-1)/2}$, where $B_m = |\mathbf{B}|_{\lambda=D}$; D and $\beta = 4.3$ denote the jet diameter and power-law spectral index of the magnetized filamentary turbulence, respectively (Honda & Honda 2007). Viewing the jet globally from outside, randomly oriented fields inside jet are cancelled, except for a large-scale toroidal magnetic field along the envelope.

As was illustrated in our previous paper (Honda & Honda 2005), there exists an energy hierarchy for protons trapped in such a filamentary current system: (i) $E_p \ll |eA|$ and (ii) $E_p \gg |eA|$, where e and A are the charge of an electron and the vector potential, respectively. The former corresponds to a low-energy regime, in which protons are strictly bounded for the local magnetic field induced by each filament. The latter reflects the higher energy regime in which the validity condition of the quasilinear approximation, $\langle f_p \rangle \gg |\delta f_p|$ is satisfied, where $\langle f_p \rangle$ and δf_p are the averaged and fluctuated part of the momentum distribution function for protons in the test-particle approximation, f_p , respectively. In this regime, protons are no longer trapped with local magnetic fields, but are deviated with small fluctuations. Below, we describe the acceleration and competitive energy losses in each energy hierarchy.

2.1. Preliminary Acceleration

In the low-energy regime of $E_p \ll |eA|$, protons are strictly bounded and gyrating around the local magnetic field induced by each filament. Energies of injected protons are elevated via the conventional diffusive shock acceleration being resonantly scattered from small magnetic fluctuations (Drury 1983). The characteristic acceleration time of protons is described by

$$t_{\text{pre,acc}} \simeq \left(\frac{3\eta_p r_{g,p}}{c} \right) \left(\frac{r-1}{r} \right), \quad (1)$$

where $\eta_p = (3/2b)(\lambda/2r_{g,p})^{2/3}$, presuming Kolmogorov turbulence, b ($\ll 1$) is the energy density ratio of fluctuating to local mean magnetic fields, $r_{g,p}$ is the proton gyroradius, and r ($=4$ for the strong shock limit) is the shock compression ratio. The achievable maximum energies of protons are limited by the various radiative cooling timescales, and here we consider two representatives: the synchrotron radiation losses, $t_{p,\text{syn}}$, and collisions with ambient photons, $t_{p\gamma}$. In blazar jets the propagation time of shock, t_{sh} , also restricts the highest energy, and hence the temporal limit is given by

$$t_{\text{pre,acc}} = \min(t_{p\gamma}, t_{p,\text{syn}}, t_{\text{sh}}). \quad (2)$$

Besides the temporal limit, there exists a spatial limit: the maximum gyroradii of protons are not allowed to exceed the transverse sizes of in-situ filaments. The achievable energy of protons

via the preliminary acceleration is determined by comparing the temporal and spatial limit. In the following, conceivable energy constraints for Mrk 501 are provided.

2.1.1. Synchrotron cooling losses

Gyrating around the filament-induced local fields, and being scattered by small fluctuations, protons emit synchrotron photons, which can be a dominant cooling process when the energy density of the magnetic field is sufficiently greater than that of the radiation. The characteristic loss time for proton synchrotron is given by (Rybicki & Lightman 1979)

$$t_{\text{p,syn}} = \frac{3m_{\text{p}}c}{4\sigma_{\text{T}}u_{\text{B}}\gamma_{\text{p}}} \left(\frac{m_{\text{p}}}{m_{\text{e}}}\right)^2 \simeq 1.2 \times 10^{13} \left(\frac{0.02 \text{ G}}{B}\right)^2 \left(\frac{10^9}{\gamma_{\text{p}}}\right) \text{ s}, \quad (3)$$

where m_{p} and m_{e} are the masses of a proton and of an electron, respectively; σ_{T} is the cross section for Thomson scattering and γ_{p} is the Lorentz factor of accelerated protons. The average energy density of the local magnetic field is denoted by $u_{\text{B}} = B^2/(8\pi)$, where $B = |\mathbf{B}|$. It should be noted that the adopted field value of $B_{\text{m}} = 0.02 \text{ G}$ (Tavecchio & Maraschi 2001) is not the one averaged over the compact blob but the maximum for a filament whose radial size is compared to the jet diameter.

2.1.2. Collisions with ambient photons

We consider proton-photon collisions leading to a pion-production cascade. Since the collision timescale is characterized by the target photon spectrum, which is still unknown, we adopt here a description by a single power-law: $n(\varepsilon_{\gamma}) \propto \varepsilon_{\gamma}^{-2}$ (Bezler et al. 1984), where $n(\varepsilon_{\gamma})$ is the number density of photons per unit energy interval $d\varepsilon_{\gamma}$. Then, the timescale can be expressed as

$$t_{\text{p}\gamma} = \chi^{-1} \left(\frac{u_{\text{B}}}{u_{\gamma}}\right) t_{\text{p,syn}} \simeq 6.0 \times 10^{10} \left(\frac{10^9}{\gamma_{\text{p}}}\right) \text{ s}, \quad (4)$$

where $u_{\gamma} \simeq 4.0 \times 10^{-4} \text{ erg cm}^{-3}$ (Bicknell et al. 2001) is the average energy density of target photon fields and $\chi \simeq 200$ (Biermann & Strittmatter 1987). Since $u_{\text{B}}/u_{\gamma} \simeq 10^{-2}$, it is found that $t_{\text{p}\gamma} \ll t_{\text{p,syn}}$.

We should also check whether collisions with particles (especially, with protons) becomes effective or not. The characteristic cooling time of relativistic protons due to inelastic pp collisions can be written as (Aharonian 2004)

$$t_{\text{pp}} = \frac{1}{n_0\sigma_{\text{pp}}fc} \simeq 1.7 \times 10^{15} \left(\frac{1 \text{ cm}^{-3}}{n_0}\right) \left(\frac{40 \text{ mb}}{\sigma_{\text{pp}}}\right) \text{ s}, \quad (5)$$

where the number density of the target hydrogen medium, $n_0 \simeq 1 \text{ cm}^{-3}$, corresponds to the upper limit assuming mass loaded hadronic jet models. The averaged total cross section, σ_{pp} , is approximately 40 mb at very high energies, and $f \simeq 0.5$ is the coefficient of inelasticity. It would be fair to say that collisions with protons should not be taken into consideration.

2.1.3. Propagation time of shock

The achievable maximum energy of protons is also restricted by the duration that the shock is propagating through the jet from the central engine to the working surface. This

corresponds to the age of a blob, which is propagating with mild-relativistic speed through the relativistic jet (Honda & Honda 2004a), and is approximately written by L/U . For Mrk 501, we obtain

$$t_{\text{sh}} = \frac{L}{U} \simeq 1.5 \times 10^9 \left(\frac{L}{7.4 \text{ pc}} \right) \left(\frac{0.5c}{U} \right) \text{ s}, \quad (6)$$

where $L \simeq 7.4 \text{ pc}$ is the distance from the core to the blob (Giovannini et al. 1999) and $U \simeq 0.5c$ is the average speed of the blob (Mücke & Protheroe 2001). This blob is currently operating for particle acceleration, and therefore t_{sh} cannot be compared to the adiabatic loss timescale for AGN, which corresponds to the lifetime of the shock (Mücke et al. 2003). The timescale of adiabatic losses is expressed as $t_{\text{ad}} = 3L/(2\Gamma_{\text{J}}v_{\text{r}})$, where Γ_{J} and v_{r} are the Lorentz factor of the jet and the speed of the radial expansion. Considering narrow opening angles of blazars, which implies $v_{\text{r}} \ll U$, we can safely say that t_{sh} is sufficiently shorter than t_{ad} .

2.1.4. Escape from local filaments

Once accelerated particles acquire sufficient energies, they are escaping from the local magnetic fields, given as a function of the filament sizes. This spatial limit is given by the assumption that the gyroradius of each particle should not be beyond the transverse size of the local filament. Then, the local maximum energy is denoted by $E_{\text{p}}^* = eBr_{\text{g,p}} \leq eB\lambda/2$.

The transverse sizes of the minimum and maximum filaments are regarded as being comparable to the Debye sheath and the jet diameter, respectively. Thus, the energy of particles escaping from the largest filament can be written as

$$E_{\text{p}}^* = \frac{eB\lambda}{2} \leq \frac{eB_{\text{m}}D}{2} \simeq 6.2 \times 10^{17} \left(\frac{B}{0.02 \text{ G}} \right) \left(\frac{D}{0.067 \text{ pc}} \right) \text{ eV}, \quad (7)$$

where $D \simeq 0.067 \text{ pc}$ is the extent of the radio emitting region (Giroletti et al. 2008). This value is estimated by substituting 0.02 G for B in the formula suggested by Marscher (1987).

2.2. Additional Acceleration

Once protons are accelerated and injected into the high-energy regime of $E_{\text{p}} \gg |eA|$, they are no longer bounded to the local magnetic field. Field vectors are randomly oriented in the internal jet in the transverse direction to the filament, and hence these protons can move almost freely in the jet being deflected by the random magnetic field. Allowing for shock propagation, protons are additionally accelerated in this regime, being off-resonantly scattered in a forest of magnetized filaments. In this aspect, the preliminary accelerator via the conventional DSA mechanism can be regarded as being an 'injector' to this further booster. The new injection mechanism is referred to as transition injection, in analogy to bound-free transition in atomic excitation. The characteristic time of the additional acceleration for protons is given by

$$t_{\text{add,acc}} = \frac{3\sqrt{6}\pi\beta r(r+1)}{8(\beta-1)(\beta_{\text{p}}+1)(\beta_{\text{p}}+2)(r-1)} \frac{cE_{\text{p}}^2}{e^2B_{\text{eff}}^2DU^2}, \quad (8)$$

where $\beta_{\text{p}} = 3$ (e.g., Stecker & Salamon 1999; de Marco, Blasi, & Olinto 2003) and $E_{\text{p}} = \gamma_{\text{p}}m_{\text{p}}c^2$

are the spectral index and energy of protons, respectively; β is the filamentary turbulent spectral index, and $|B_{\text{eff}}|^2/B_m^2 \sim 0.5$ is assumed. The maximum energy boosted by the additional acceleration is also restricted by some radiative loss processes. In addition to two possible timescales: for diffuse synchrotron, $t_{\text{d,syn}}$, and for the $p\gamma$ collision, $t_{\text{d,p}\gamma}$, we consider the shock propagation timescale, t_{sh} , and therefore $t_{\text{add,acc}} = \min(t_{\text{d,syn}}, t_{\text{d,p}\gamma}, t_{\text{sh}})$. The spatial limit will also be considered.

2.2.1. Diffuse synchrotron losses

The additionally accelerated protons deflected by the random magnetic fields emit unpolarized synchrotron radiation. Here, we adopt the characteristic cooling time for the diffuse synchrotron from our previous paper (Honda & Honda 2007), which was derived from the theoretical basis by Toptygin & Fleishman (1987):

$$t_{\text{d,syn}} = \frac{3m_p c}{4\sigma_T u_B \gamma_p} \left(\frac{m_p}{m_e}\right)^2 \frac{1}{36\pi^2} \frac{\beta(\beta+2)^2(\beta+3)}{2^\beta(\beta^2+7\beta+8)} = t_{\text{p,syn}} \tilde{\tau}(\beta), \quad (9)$$

where $t_{\text{p,syn}}$ is the timescale of normal synchrotron losses and $\tilde{\tau}(\beta) \equiv (6\pi)^{-2}[\beta(\beta+2)^2(\beta+3)/2^\beta(\beta^2+7\beta+8)]$. For $\beta = 4.3$ (Honda & Honda 2007), the maximum energy of a proton, γ_p , is directly estimated by the equation $t_{\text{add,acc}} = t_{\text{d,syn}}$, which gives

$$\gamma_p \simeq 2.7 \times 10^{11} \left(\frac{U}{0.5c}\right)^{2/3} \left(\frac{D}{0.067 \text{ pc}}\right)^{1/3}. \quad (10)$$

It should be noted that the maximum energy restricted by the diffuse synchrotron is free from the magnetic field strength because of the same B -dependence of $t_{\text{add,acc}}$ and $t_{\text{d,syn}}$.

2.2.2. Energy losses due to $p\gamma$ collision

Cooling due to collisions with photons is also characterized by the above-mentioned diffuse synchrotron: $t_{\text{d,p}\gamma} = \chi^{-1}(u_B/u_\gamma)t_{\text{d,syn}}$. Using the same target photon spectrum and other notation with those given in §2.1.2, we obtain

$$\gamma_p \simeq 4.6 \times 10^{10} \left(\frac{U}{0.5c}\right)^{2/3} \left(\frac{D}{0.067 \text{ pc}}\right)^{1/3}. \quad (11)$$

2.2.3. Restriction from the Age of the Blob

As we have mentioned in §2.1.3, the shock propagation time regarded as the age of the blob restricts the acceleration. Equating $t_{\text{add,acc}} = t_{\text{sh}}$, we obtain

$$\gamma_p \simeq 4.3 \times 10^9 \left(\frac{U}{0.5c}\right)^{1/2} \left(\frac{L}{7.4 \text{ pc}}\right)^{1/2} \left(\frac{D}{0.067 \text{ pc}}\right)^{1/2}. \quad (12)$$

2.2.4. Spatial Limit for Additional Acceleration

It should be noted that additionally accelerated particles are not gyrating to the local fields, but deflected by randomly oriented fields. Thus, the spatial limit is determined by the condition that the mean free path for this collisionless deflection should be smaller than the system size: $\ell \sim \tilde{\rho}D$, where $\tilde{\rho} > 1$ is a dimensionless parameter (see, Honda & Honda 2005, for the details). It gives

$$\begin{aligned}
E_p^{\max} &= \sqrt{\frac{2(\beta - 1)(\beta_p + 2)(\beta_p + 4)\psi_1^2}{\pi\beta}} \tilde{\rho}^{1/2} e B_{\text{eff}} D \\
&\simeq 2.1 \times 10^{18} \left(\frac{B_{\text{eff}}}{0.014 \text{ G}} \right) \left(\frac{D}{0.067 \text{ pc}} \right) \text{ eV},
\end{aligned} \tag{13}$$

where $\tilde{\rho} = 1$ is assumed.

2.3. Achievable Maximum Energy of Protons

Putting together the above discussion, provided both the normal and transition injection of protons are realized in a blazar jet, multi-stage diffusive shock acceleration can take place. In this subsection, we present the results of a numerical evaluation of the achievable maximum energies of protons in both stages within the conceivable parameter region. In Fig.1, the energies of accelerated protons are plotted against the transverse filament size parametrizing the ratio of the mean/fluctuate magnetic energy density, b . The transverse filament sizes, λ , covers the range from 10^{-4} pc to 0.067 pc. The minimum and the maximum sizes are compared to the correlation length of Alfvénic fluctuation and the jet diameter, respectively. As shown, in the case of preliminary acceleration the achievable maximum energies of protons are mainly restricted by the escape from individual filaments, which is represented by a linearly increasing line ($\propto \lambda^{2.65}$). In the case of $b = 10^{-2}$, the proton energies achieved via preliminary acceleration, E_p^* , are determined by $r_{g,p} \leq \lambda$ over the whole range of the considered filament sizes. In the case of $b = 10^{-3}$, the values of E_p^* are also determined by $r_{g,p} \leq \lambda$ for $\lambda < 1.7 \times 10^{-2}$ pc, while the E_p^* -values are more severely restricted by the propagation time of the shock for $\lambda \geq 1.7 \times 10^{-2}$ pc, and hence the achievable energy via the preliminary acceleration, E_p^* , is cut-off at 10^{16} eV. If $b \leq 10^{-4}$, the E_p^* -values are perfectly overlapped with those of $b = 10^{-2}$. On the other hand, the maximum energy achieved by the additional acceleration E_p^{\max} is independent of not only the filament size, but also the b -parameter. The energies of accelerated protons can be additionally boosted up to the value determined by the spatial limit expressed with a horizontal line of $E_p^{\max} = 2.1 \times 10^{18}$ eV, irrespective of their energies acquired by the preliminary acceleration.

We also present the λ -dependence of E_p^* parametrizing the B_m -value in Fig.2. The lines corresponding to $r_{g,p} = \lambda$ shift upwards with a larger B_m . For the cases of $B_m = 0.01$ G and 0.1 G, the proton energies achieved by the preliminary acceleration, E_p^* , are determined by $r_{g,p} \leq \lambda$ over the whole range of conceivable filament sizes. In the cases of $B_m = 1$ G and 10 G, the protons dominantly lose their energies via collisions with photons for $\lambda \geq 4.2 \times 10^{-2}$ pc and for $\lambda \geq 1.5 \times 10^{-2}$ pc, respectively. Thus, the resultant maximum value of E_p^* is nearly 10^{19} eV. As for the additional acceleration, the E_p^{\max} -values are expressed by horizontal lines because of their independence of λ . The lowest and the highest E_p^{\max} correspond to those of $B_m = 10^{-2}$ G and $B_m = 10^{-1}$ G, respectively, and in both cases the maximum energies are restricted by the spatial limit. The E_p^{\max} -value for $B_m = 1$ G is identical to that for $B_m = 10$ G, and in these cases the energy is restricted by collisions with ambient photons.

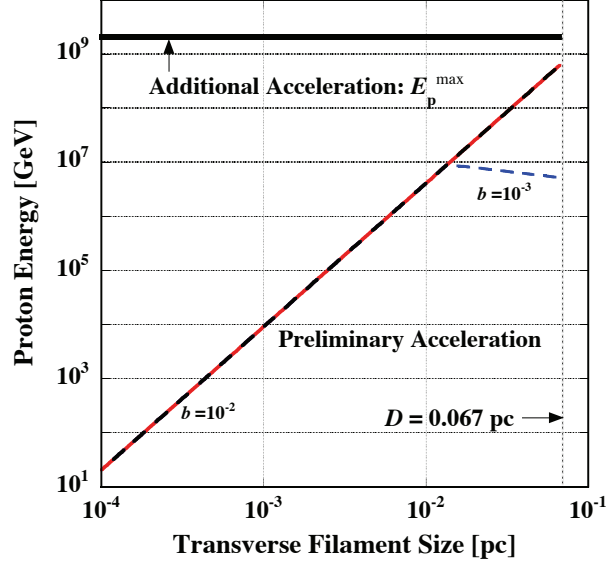


Fig. 1. Maximum energies of accelerated protons versus the transverse filament sizes for various b -values. The value of B_m is fixed at 0.02 G. The monotonically increasing line and its branch denote the maximum energies achieved by the preliminary acceleration. Solid and dashed lines correspond to the cases of $b = 10^{-2}$ and 10^{-3} , respectively. The horizontal bold line denotes the maximum energy achieved by additional acceleration.

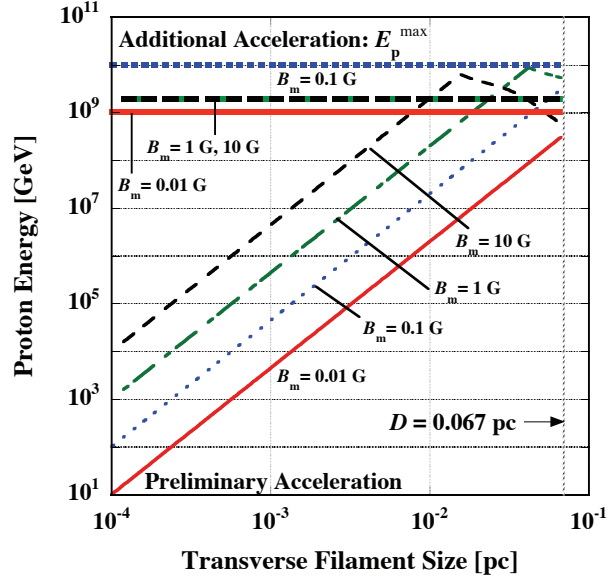


Fig. 2. Maximum proton energies versus the transverse filament sizes for various B_m -values. The value of b is fixed at 10^{-3} . Four monotonically increasing lines denote the limitations obtained by preliminary acceleration. The cases of $B_m = 0.01$ G, 0.1 G, 1 G, and 10 G are plotted by solid, dotted, dot-dashed, and dashed curves, respectively. Horizontal thick lines represent the cutoff energies achieved by additional acceleration. The line types are the same as those for preliminary acceleration.

3. Estimation of the Neutrino Flux from Mrk 501

In the previous section we calculated the achievable maximum energies of protons in a blazar jet. Since the proton energies accelerated by multi-stage DSA are sufficiently higher than the neutrino-producing threshold via photopionization, we can safely expect significant fluxes of energetic neutrinos.

3.1. Neutrino Energies Produced by Accelerated Protons

In the photomeson process of $p\gamma \rightarrow \Delta^{++} \rightarrow \pi^+ N$, the center-of-mass energies of accelerated protons should be beyond the Δ -resonance threshold, $m_\Delta = 1230$ MeV,

$$E_p^{\min} = \Gamma_J^2 \frac{m_\Delta^2 - m_p^2}{4E_\gamma}, \quad (14)$$

where Γ_J and E_γ are the Lorentz factor of a blazar jet and the mean energy of ambient photons, respectively. Presuming that the generated pion energy is equally divided into four leptons through the decay $\pi^+ \rightarrow \nu_\mu \mu^+ \rightarrow \nu_\mu e^+ \nu_e \bar{\nu}_e$, the neutrino energy is described as

$$E_\nu = \frac{1}{4} \langle x_{p \rightarrow \pi} \rangle E_p, \quad (15)$$

where $\langle x_{p \rightarrow \pi} \rangle \simeq 0.2$ is the averaged fraction of momentum transfer from a proton to a pion.

As for the Mrk 501, the peak energy of synchrotron emission in the X-ray band is shifted from 1 keV to 100 keV during flaring (Kataoka et al. 2001). Since these energies are achievable for synchrotron photons emitted from co-accelerated electrons, we take these values as the mean energy of ambient photons. For $E_\gamma = 100$ keV, we obtain the neutrino producing threshold using eq.(14) as

$$E_p^{\min} = 1.4 \left(\frac{\Gamma_J}{30} \right)^2 \left(\frac{100 \text{ keV}}{E_\gamma} \right) \text{ PeV}, \quad (16)$$

which leads to $E_p^{\min} = 70$ TeV. Similarly, for $E_\gamma = 1$ keV, $E_p^{\min} = 140$ PeV and hence $E_\nu^{\min} = 7$ PeV. Since the maximum energy of accelerated protons is sufficiently higher than these threshold values, Mrk 501 can be a feasible source of neutrinos. In both cases we determined $E_\nu^{\max} \simeq 110$ PeV, according to the upper limit estimated in §2.3.

3.2. Energetic Neutrino Flux from Mrk 501

In order to calculate the neutrino flux produced at an individual blazar, we begin with the following useful formula:

$$\int_{E_\nu^{\min}}^{E_\nu^{\max}} E_\nu \frac{d\Phi}{dE_\nu} dE_\nu = \frac{L_\nu}{4\pi d_L^2}, \quad (17)$$

where the upper and lower limits of integration are the maximum and minimum (threshold) neutrino energies, estimated in §3.1, respectively. The luminosity distance to the blazar, d_L , is defined as

$$d_L = d_m(1+z) = \frac{c(1+z)}{H_0} \int_0^z \sqrt{(1+z)^2(1+\Omega_m z) - z(2+z)\Omega_\Lambda} dz, \quad (18)$$

where z is the redshift ($=0.034$ for Mrk 501: Quinn et al. 1996) for Mrk 501 and d_m is the proper motion distance, which is written by the Hubble constant, $H_0 = 71 \text{ km}^{-1}\text{Mpc}^{-1}$, the matter density, $\Omega_m = 0.27 \pm 0.04$, and dark energy density, $\Omega_\Lambda = 0.73 \pm 0.04$, adopted from WMAP results (Bennett et al. 2003).

The observed neutrino luminosity, L_ν , is defined as

$$L_\nu = \frac{N_\nu \langle E_\nu \rangle}{\Delta t_{\text{obs}}}, \quad (19)$$

where N_ν , $\langle E_\nu \rangle$, and $\Delta t_{\text{obs}} \simeq 1 \text{ d}$ are the number of produced neutrinos, the mean neutrino energy, and the observed variability time of the emission region, respectively. Since N_ν and $\langle E_\nu \rangle$ are not observables, we introduce the optical depth defined as

$$\tau = R n_\gamma \sigma_{p\gamma \rightarrow \Delta} = R \frac{L_\gamma \Delta t_{\text{obs}}}{V \langle E_\gamma \rangle} \sigma_{p\gamma \rightarrow \Delta}, \quad (20)$$

where $L_\gamma \simeq 10^{45} \text{ erg/s}$ is the observed photon luminosity, V represents the volume of emission region with radius R , $\langle E_\gamma \rangle \simeq 10 \text{ eV}$ denotes the mean energy of photons, and $\sigma_{p\gamma \rightarrow \Delta} \simeq 10^{-28} \text{ cm}^2$ is the Δ -resonance photopionization cross section. Then, we can express L_ν with observable quantities in a compact notation,

$$L_\nu = K \tau L_p = K \tau e^\tau L_{p,\text{obs}}, \quad (21)$$

where $K \simeq 0.024$ is a constant taking the branching ratios of interaction chain and corresponding momentum transfer into account. The intrinsic proton luminosity, L_p , can be replaced with the observed $L_{p,\text{obs}}$ taking the proton interactions with ambient photons into consideration. However, $L_{p,\text{obs}}$ is still unknown; we assume it to be as 10 % of the photon total luminosity (Halzen & Hooper 2002). We also replace τ with $(1 - e^{-\tau})$, with considering the possible p and π^+ absorption in the vicinity of the source.

Summarizing the above discussion, we adopt the following formula of differential flux from an individual blazar (Bazo & Gago 2005):

$$\frac{d\Phi_{\nu_\mu + \bar{\nu}_\mu}}{dE_\nu} = \frac{2^{0.1} K L_\gamma (1 - e^{-\tau}) e^{(1 - e^{-\tau})}}{4\pi d_L^2} E_\nu^{-p} \exp\left(-\frac{E_\nu}{E_{\text{cut}}^{\text{AGN}}}\right), \quad (22)$$

where the factor 2 reflects the contribution of neutrinos and anti-neutrinos. Since we are concerned with the point-source neutrino flux, we consider the ν_μ contribution on account of their highest angular resolution. This is attributed to the large muon track, having advantage of reconstructing paths.

In Fig.3 we plot the differential flux of neutrinos from Mrk 501 against their energies. The energy of neutrinos is limited to the range between the maximum and the minimum predicted by this model. Here, we adopt the typical power-law energy distribution of neutrinos, E_ν^{-p} , with the exponential cutoff, $E_{\text{cut}}^{\text{AGN}}$. We parametrize the power-law index $p = 1.3, 2.0, 2.7$, where

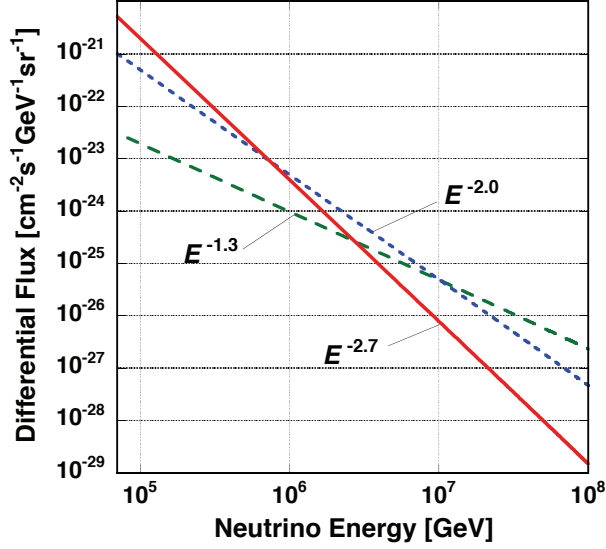


Fig. 3. Differential neutrino flux from a blazar jet of Mrk 501 versus neutrino energy. The power-law energy distribution of neutrinos, E_ν^{-p} , with an exponential cutoff $E_{\text{cut}}^{\text{AGN}} = 2.1 \times 10^{18}$ eV is assumed. The power-law indices of $p = 1.3$, 2.0, 2.7 are denoted by the dashed, dotted, and solid curves, respectively.

$p = 1.3$ and $p = 2.7$ are taken from the upper and lower limits of the exponents, respectively, and $p = 2.0$ is a resemblance of the parent proton spectrum supposed to be accelerated by Fermi's mechanism. The cutoff energy, $E_{\text{cut}}^{\text{AGN}} = 2.1 \times 10^9$ GeV, is the achievable maximum energy of AGN protons estimated in §2.3. One can see that for a steeper energy spectrum the neutrino flux is more significantly reduced in the energy range of $E_\nu \gtrsim 10^8$ GeV. On the contrary, in the lower energy region of $E_\nu \lesssim 10^6$ GeV the flux is higher in the case of a steeper spectrum because of the contribution from the denominator. Anyhow, the neutrino flux originating from a single blazar is trivial compared to the observable level.

3.3. Calculation of the ν_μ -Induced Event Number

It is more difficult to detect higher energy neutrinos because of the steeply falling spectrum. In order to detect the interaction of a TeV neutrino with a Cherenkov telescope, the effective volume of the detector is required for kilometer scale to cover the typical range of TeV muons. In the effective region of the telescope, the probability to detect ν_μ in the TeV-PeV range is approximately given by

$$P_{\nu_\mu \rightarrow \mu} \simeq \frac{R_\mu}{\lambda_{\text{int}}} \simeq 1.3 \times 10^{-6} \left(\frac{E_\nu}{1 \text{ TeV}} \right)^{0.8}, \quad (23)$$

where R_μ and λ_{int} are the muon range and the neutrino interaction length, respectively (Gaisser, Halzen, & Stanev 1995).

We can now compute the diffuse neutrino event rate by integrating the total differential flux multiplied by the detection probability of eq.(23)

$$N_{\nu_\mu} = \int_{E_\nu^{\min}}^{E_\nu^{\max}} dE_{\nu_\mu} \left\langle \frac{d\Phi_{\nu_\mu}(E_{\nu_\mu})}{dE_{\nu_\mu}} \right\rangle_{\text{tot}} P_{\nu_\mu \rightarrow \mu}, \quad (24)$$

where the upper and lower limits of the integral are $E_\nu^{\max} \simeq 1.1 \times 10^{17}$ eV and $E_\nu^{\min} \simeq 7 \times 10^{13}$ eV calculated in § 3.1, respectively. In order to compute the diffuse neutrino flux from the observed blazar distribution, we should integrate the flux from all blazars while taking the Doppler factor distribution into consideration. For simplicity, here we adopt the effective number of blazars (Halzen & Zas 1997), using the γ -ray flux ratio of diffuse to the single blazar, which is derived from the luminosity function of 20 brightest blazars obtained by the EGRET collaboration (Chiang et al. 1995). Thus, instead of summing up the total isotropic differential flux of neutrinos $\left\langle \frac{d\Phi_{\nu_\mu}}{dE_{\nu_\mu}} \right\rangle_{\text{tot}}$, we simply estimate the diffuse flux by multiplying the flux of Mrk 501 by the resultant number 130 sr^{-1} . A correction for the difference in the spectral indices of gamma-ray and neutrino fluxes enhances the neutrino flux by a factor of three. We present the estimated neutrino event rates in Table 1 for conceivable power-law exponents. Considering the 4π coverage and typical exposure time (~ 10 yr), the value $N_{\nu_\mu} \simeq 2 \text{ km}^{-2} \text{ yr}^{-1}$ sufficiently reaches to the observable level.

Table 1. Neutrino event rates for various power-law exponents.

Power-law exponent	Event rate
$p = 1.3$	0.78
$p = 2.0$	1.3
$p = 2.7$	1.9

4. Conclusions

In this paper we applied our model of multi-stage diffusive shock acceleration to the blazar Mrk 501 and evaluated the maximum energies of protons. We also calculated the neutrino flux from this single source generated by these accelerated protons, and discuss the detectability with the updated neutrino telescope, IceCube. We obtained the EeV protons and differential flux during the operating time of the detector by not a simple, optimistic order estimation, but by considering the systematical energy restriction at the source. The results are rather sensitive to the values of the magnetic field strength and the size of the accelerator. The B -field value is related to the system size via the radiation intensity of the emission region. In the conceivable range of the field strength, EeV protons are obtained by additional acceleration.

Y. S. H. thanks K. Murase for useful comments.

References

- Abbasi, R. et al. 2009, Phys. Rev. D, 79, 062001
- Abraham, J. et al. (The Pierre Auger Collaboration) 2007, Science, 318, 938
- Aharonian, F. A. 2004, in Very High Energy Cosmic Gamma Radiation: A Crucial Window on the Extreme Universe (Singapore: World Scientific), 109
- Appl, S., & Camenzind, M. 1992, A&A, 256, 354
- Bazo, J. L., & Gago, A. M. 2005, arXiv: astro-ph/0504554
- Bennett, C. L., et al. 2003, ApJS, 148, 97
- Bezler, M., Kendziorra, E., Staubert, R., Hasinger, G., Pietsch, W., Reppin, C., Trümper, J., & Voges, W. 1984, A&A, 136, 351
- Bhattacharjee, P., & Sigl, G. 2000, Phys. Rep., 327, 109
- Bicknell, G. V., Wagner, S. J., & Groves, B. 2001, in Proc. AIP Conf., 558, 261
- Biermann, P. L., & Strittmatter, P. A. 1987, ApJ, 322, 643
- Biretta, J. A., Owen, F. N., & Hardee, P. E. 1983, ApJ, 274, L27
- Blandford, R., & Eichler, D. 1987, Phys. Rep., 154, 1
- Blazejowski, M., et al. 2005, ApJ, 630, 130
- Capetti, A., Macchetto, F. D., Sparks, W. B., & Biretta, J. A. 1997, A&A, 317, 637
- Carilli, C. L., & Barthel, P. D. 1996, A&A Rev., 7, 1
- Catanese, M., et al. 1997, ApJ, 487, L143
- Catanese, M., & Sambruna, R. M. 2000, ApJ, 534, L39
- Chiang, J., Fichtel, C. E., von Montigny, C., Nolan, P. L., & Petrosian, V. 1995, ApJ, 452, 156
- Cui, W. 2004, ApJ, 605, 662
- de Marco, D., Blasi, P., & Olinto, A. V. 2003, Astroparticle Phys., 20, 53
- Drury, L. O 'C. 1983, Rep. Prog. Phys., 46, 973
- Fossati, G., et al. 2000, ApJ, 541, 153
- Fraschetti, F., & Melia, F. 2008, MNRAS, 391, 1100
- Gabuzda, D. C. 1999, NewAstron. Rev. 43, 691
- Gaisser, T. K., Halzen, F., & Stanev, T. 1995, Phys. Rep., 258, 173; [Erratum: 1995, Phys. Rep., 271, 355]
- Giovannini, G., Feretti, L., Venturi, T., Cotton, W. D., & Lara, L. 1999, in ASP Conf. Ser. 159, ed. L. O. Takalo & A. S. Silanpää (San Fransisco ASP), BL Lac Phenomenon, a conference held 22-26 June 1998 in Turku, Finland, 439
- Gioiretti, M., Giovanni, G., Cotton, W. D., Taylor, G. B., Pérez-Torres, M. A., Chiaberge, M., & Edwards, P. G., 2008, A&A, 488, 905
- Halzen, F., & Hooper, D. 2002, Rep. Prog. Phys. 65, 1025
- Halzen, F., Landsman, H., & Montaruli, T. 2005, arXiv: astro-ph/0503348
- Halzen, F. 2005, Lectures presented at the International WE Heraeus Summer School on Physics with Cosmic Accelerators [arXiv: astro-ph/0506248]
- Halzen, F., & Hooper, D. 2005, Astroparticle Phys., 23, 537
- Halzen, F., & Zas, E. 1997, ApJ, 488, 669
- Honda, M., & Honda, Y. S. 2002, ApJ, 569, L39

- Honda, Y. S., & Honda, M. 2004a, ApJ, 613, L25
Honda, M., & Honda, Y. S. 2004b, ApJ, 617, L37
Honda, M. 2004, Phys. Rev. E, 69, 016401
Honda, M., & Honda, Y. S. 2005, ApJ, 633, 733
Honda, M., & Honda, Y. S. 2007, ApJ, 654, 885
Honda, M. 2008, ApJ, 675, L61
Honda, M. 2009, ApJ, 706, 1517
IceCube Collab. 2004, Astropart. Phys., 20, 507
Ioka, K., Razzaque, S., Kobayashi, S., & Mészáros, P. 2005, ApJ, 633, 1013
Kataoka, J., et al. 2001, arXiv: astro-ph/0105029
Kazimura, Y., Sakai, J. I., Neubert, T., & Bulanov, S. V. 1998, ApJ, 498, L183
Kotani, T., Kawai, N., Matsuoka, M., & Brinkmann, W. 1996, PASJ, 48, 619
Koyama, K., Petre, R., Gotthelf, E. V., Hwang, U., Matsuura, M., Ozaki, M., & Holt, S. S. 1995, Nature, 378, 255
Krawczynski, H., Coppi, P. S., Maccarone, T., & Aharonian, F. A. 2000, A&A, 353, 97
Lagage, P. O., & Cesarsky, C. J. 1983, A&A, 118, 223
Lagage, P. O., & Cesarsky, C. J. 1983, A&A, 125, 249
Marscher, A. P. 1987, in Superluminal Radio Sources, ed. J. A. Zensus & T. J. Pearson (Cambridge: Cambridge University Press), 280
Meisenheimer, K., Röser, H. -J., Hiltner, P. R., Yates, M. G., Longair, M. S., Chini, R., & Perley, R. A. 1989, A&A, 219, 63
Mücke, A., & Protheroe, R. J. 2001, Astroparticle Phys. 15, 121
Mücke, A., Protheroe, R. J., Engel, R., Rachen, J. P., & Stanev, T. 2003, Astroparticle Phys. 18, 593
Nan, R. D., Zhang, H. Y., Gabuzda, D. C., & Inoue, M. 1999, PASJ, 51, 955
Nishikawa, K. -I., Hardee, P., Richardson, G., Preece, R., Sol. H., & Fishman, G. J. 2003, ApJ, 595, 555
Novak, G., et al. 2003, ApJ, 583, L83
O'Sullivan, S., Reville, B., & Taylor, A. M. 2009, MNRAS, 400, 248
Perley, R. A., Dreher, J. W., & Cowan, J. J. 1984, ApJ, 285, L35
Pian, E., et al. 1998, ApJ, 492, L17
Quinn, J., et al. 1996, ApJ, 456, L83
Rawlings, S., & Saunders, R. 1991, Nature, 349, 138
Rybicki, G. B., & Lightman, A. P. 1979, Radiative Processes in Astrophysics (New York: Wiley-Interscience), ch.6
Rebillot, P. F., et al. 2006, ApJ, 641, 740
Sambruna, R. M., et al. 2000, ApJ, 538, 127
Sembay, S., Edelson, R., Markowitz, A., Griffiths, R. G., & Turner, M. J. L. 2002, ApJ, 574, 634
Silva, L. O., Fonseca, R. A., Tonge, J. W., Dawson, J. M., Mori, W. B., & Medvedev, M. V. 2003, ApJ, 596, L121
Stecker, F. W., & Salamon, M. H. 1999, ApJ, 512, 521
Takahashi, T., et al. 1996, ApJ, 470, L89

- Tavecchio, F., & Maraschi, L. 2001, in AIP Conf. Proc., 599, X-ray Astronomy: Stellar Endpoints, AGN, and the Diffuse X-ray Background, ed. N. E. White, G. Malaguti, & G. G. C. Palumbo, (New York: AIP), 979
- Toptygin, I. N., & Fleishman, G. D. 1987, Ap&SS, 132, 213
- Vietri, M. 1998, Phys. Rev. Lett., 80, 3690
- Waxman, E., & Bahcall, J. 1997, Phys. Rev. Lett., 78, 2292
- Woschnagg, K., for the AMANDA Collaboration, 2005, Nucl. Phys. B, Proc. Suppl. 143, 343